Modeling the Chandra High Energy Transmission Gratings below 2 keV

K.A. Flanagan[a], T.H. Markert[a], J.E. Davis[a], M.L. Schattenburg[a], R.L. Blake[b], F. Scholze[c], P. Bulicke[c], R. Fliegauf[c], S. Kraft[c], G. Ulm[c], E.M. Gullikson[d]

[a]Center for Space Research
Massachusetts Institute of Technology, Cambridge, MA, 02139

[b]RDS, P.O. Box 6880, Santa Fe, NM, 87502

[c]Physikalisch-Technische Bundesanstalt
Abbestr. 2-12, 10587 Berlin, Germany

[d]Center for X-Ray Optics
Lawrence Berkeley National Laboratory, Berkeley, CA 94720

ABSTRACT

The High Energy Transmission Grating Spectrometer of the *Chandra* X-Ray Observatory is a high spectral resolution instrument utilizing gold X-ray transmission gratings. The gratings have been subjected to a rigorous program of calibration, including testing at synchrotron facilities for the purpose of refining and testing the grating model. Here we conclude our investigation of the optical constants of gold, extending it below 2 keV to complete the coverage over the *Chandra* energy range. We investigate the carbon, nitrogen, oxygen and chromium edge structures introduced by the grating support membrane. Finally, we summarize the state of the grating model, identifying those energy regions where the residuals are most significant and suggesting where the model might be improved.

Keywords: X-ray, X-ray astronomy, X-ray spectroscopy, transmission gratings, diffraction, synchrotron, scattering factor, index of refraction

1. INTRODUCTION

The High Energy Transmission Grating Spectrometer (HETGS) of the *Chandra* X-Ray Observatory is a high spectral resolution instrument including 336 gold X-ray transmission gratings. The instrument is described in Markert *et al.*.[1] The gratings have been subjected to a rigorous program of calibration testing with a goal of modeling the first order efficiency to 1% outside of absorption edges. The gratings are of two types: High Energy Gratings (HEG) and Medium Energy Gratings (MEG), which consist of gold bars (of 2000 Å and 4000 Å periods, respectively) atop polyimide support membranes. Details of fabrication are given in Schattenburg *et al.*[2]

Calibration of the *Chandra* High Energy Transmission Gratings has involved several distinct phases: (1) Subassembly calibration, including laboratory testing of each flight grating facet against transfer standard gratings[3,4]; (2) synchrotron facility testing of selected gratings and sample foils and filters[5,6,7,8]; (3) testing of the assembled instrument at the Marshall Space Flight Center, including end-to-end testing with the flight optics and detectors[9,10,11,12,13,14,15]; and (4) in-flight calibration.[16]

The synchrotron radiation measurements serve several purposes. Transmission measurements of polyimide, plating base and gold foil samples allow the optical constants and edge structures of these materials to be determined. Absolute efficiency measurements of a few gratings serve to validate and constrain our model, and provide estimates of its intrinsic errors. Measurements of individual gratings HX220 and MX078 have enabled their use as transfer standards in laboratory tests. Finally, a comparison of synchrotron measured efficiencies of a few gratings with their predicted efficiencies based on laboratory measurements allows us to assess the limitations of our subassembly tests.

Further author information: (Send correspondence to K.A.F.)
K.A.F.: E-mail: kaf@space.mit.edu

X-Ray and Gamma-Ray Instrumentation for Astronomy XI, Kathryn A. Flanagan, Oswald H. W. Siegmund, Editors, Proceedings of SPIE Vol. 4140 (2000) © 2000 SPIE · 0277-786X/00/$15.00

The present paper addresses the first two of these purposes. Here we complete our revision of the optical constants of gold and our characterization of the edge structure of the materials in the support membrane. The revised grating model, which incorporates this new information, is then compared against detailed synchrotron radiation measurements on two flight gratings. Since these measurements provide efficiencies at hundreds of energies, we have a clear picture of the overall fidelity of the model and a practical estimate of its limitations. These tests, and their results, are described below.

1.1. Components of the Grating Model

We view the "grating model" from a calibration point of view: Our ability to fit measured grating efficiencies with a model will depend on our input data, as well as on our understanding of the grating physics. As we shall see in Section 4, the largest remaining discrepancies between the measurements and the model are at the absorption edges. Our measurements of the optical constants at these edges has greatly improved our model, yet this input data set is still the limiting factor overall. Nevertheless, some areas invite investigation at the conceptual level as well.

The model we use for the diffraction efficiency is based on the simple scalar (Kirchhoff) diffraction theory.[17] A discussion of some aspects of the model is given in Markert *et al.*.[7] Apart from diffraction by the grating bars, other factors affect the measured efficiency of the gratings and are included in the model. These include the absorptions of the film and the plating base. The grating is built up onto a thin (0.98 μm for the HEGs, 0.55 μm for the MEGs) polyimide film which provides mechanical support. In addition, there are very thin metallic films ($\simeq$ 200 Å of gold and 50 Å of chromium) which are used for the electroplating process. These films are essentially uniform over the grating and serve only to absorb (and not diffract) X-rays. However, their absorption introduces edge structure which will be discussed in detail in this paper.

A full specification of our grating model includes the grating bar shape, the thicknesses of the plating base and support polyimide support film, as well as the energy-dependent optical constants for the gold, polyimide and chromium. The geometric components are regarded as parameters to be deduced from a fitting procedure. Hence, the model consists of the following:

$\beta_{au}(k)$ and $\delta_{au}(k)$, the components of the index of refraction for gold
$z(\xi)$, the bar shape function
t_{au}, the thickness of the gold plating base
t_{cr}, the thickness of the chromium plating base
t_{poly}, the thickness of the polyimide support film
$\beta_{polyimide}(k)$ and $\beta_{cr}(k)$, the imaginary parts of the index of refraction, which give the transmissions of the support film and the plating base, and
A, the amplitude factor.

The *amplitude factor* accounts for grating imperfections which affect the measured diffraction efficiencies. One example of a factor which can affect measured diffraction efficiency is grating scatter.[15] The observations of scatter are compatible with fluctuations in grating bar geometry. Other factors may also be considered, such as minute pinholes or small regions which are non-diffracting. Since each of these affects the relative measurements of zero and higher order efficiencies, we use a multiplicative factor (the amplitude factor) to account for this in modeling the efficiency of each order.

The optical constants are not fitted as free parameters: There are too many (2 at each energy for gold alone), so fitting them isn't appropriate. Any errors in these values will be manifested in the fit, and will significantly impact our ability to accurately model the first order efficiencies. Therefore, we have employed synchrotron transmission tests to provide independent information about the optical constants of the grating and plating base materials ($\beta_{au}(k)$, $\delta_{au}(k)$, $\beta_{polyimide}(k)$ and $\beta_{cr}(k)$). Prior measurements are described in Section 1.2. Revisions to the gold constants below 2 keV are described in Section 2; revisions to the constants for polyimide and chromium are described in Section 3.

In practice, when fitting a model to an individual grating, we allow all parameters to vary except for the optical constants. The bar shape function may be thought of as the cross-section of the grating bar for X-rays normally incident on the grating surface. It is taken to be piece-wise linear, nominally with five vertices. There are two free parameters to fix the positions of each vertex. The plating base components and amplitude factor each provide another free parameter, totaling 14 when a model with five vertices is employed.

This model has been compared against detailed synchrotron radiation measurements on two flight quality gratings, HA2021 and MA1047. This gives us a practical measure of the validity and limitations of the grating model. These tests, and their results, are described in Section 4.

1.2. Summary of Synchrotron Radiation Tests

Synchrotron radiation tests for the High Energy Transmission Gratings have been performed at four facilities over a timeframe of several years. The tests are summarized in Table 1. Our earliest modeling efforts were based upon a rectangular grating bar model and employed scattering factors (f1, f2) published by Henke *et al.*.[18] (The real and imaginary parts of the index of refraction, δ and β, are obtained from the scattering factors.) However, early tests (January 1994) at the National Synchrotron Light Source (NSLS) at Brookhaven National Laboratory (BNL) indicated significant disagreement with the Henke values for the gold optical constants. The most noticeable feature was that the energies of the gold M absorption edges were shifted from the tabulated amounts by as much as 40 eV (a result obtained earlier by Blake *et al.*[19] from reflection studies of gold mirrors.) In an effort to determine more relevant optical constants, the transmission of a gold foil was measured over the range 2.03–6.04 keV, and the values of β and δ were revised.[6] (The Henke tables were modified in 1996 to reflect these results.)

Subsequent tests on gratings explored bar shape, tilt and asymmetry,[7] and tests at the radiometry laboratory of the Physikalish-Technische Bundesanstalt (PTB) below 2 keV identified the need to accurately model the edge structures of the polyimide support membrane to improve the overall fit.[8] The analysis of the tests performed on gold and polyimide membranes at PTB in October 1995 has now been completed and is detailed in Sections 2 and 3. As a consequence of this analysis, our model now includes revised gold optical constants over the full energy range appropriate to HETG, and detailed structure for absorption edges of C, N, O and Cr. In addition, cross-checks of the revised gold constants (above 2 keV) and polyimide were performed (in August and November, 1996) and have confirmed our revisions. For reference, the revision date for these changes to our modeling is May 10, 1999.

Table 1. Summary of HETG synchrotron radiation tests

Date	Facility	Sample	Energy	Comments	Ref.
July '93	NSLS	HX101	2.03 - 4	preliminary tests	Nelson[5]
Nov '93	Daresbury	HX101	8.442	period variations (UL)	Nelson[5]
Jan. '94	NSLS	HX101	0.7 - 6	first tests	Nelson[6]
Feb. '94	NSLS	1Au	2.03 - 6.04	gold optical constants	Nelson[6]; also †
Jun. '94	NSLS	HA04	2.03 - 6		Nelson[6]
"	"	HX101	2 - 3.5		Nelson[6]
"	"	MA12	0.7 - 5	±1 order assymetry	Nelson[6]
Feb. '95	NSLS	HX220	0.5 - 6.4	X-GEF reference grating	Markert[7]
"	"	MX078	0.5 - 3.5	X-GEF reference grating	Markert[7]
May '95	NSLS	HX220	1.05 - 1.95	X-GEF reference grating	Markert[7]
"	"	poly	0.4 - 1.83	poly transmission	this paper*
Oct. '95	NSLS	HA2021	2.03 - 6.5	flight lot 2, dense 0&1 orders	Flanagan[8]
"	"	MA1047	2.1 - 5.0	flight lot 3, dense 0&1 orders	Flanagan[8]
Oct. '95	PTB	HA2021	0.4 - 1.9	flight lot 2	Flanagan[8]
"	"	MA1047	0.4 - 1.5	flight lot 3	Flanagan[8]
"	"	HA2049	0.2 - 1.5	polyimide sample, flight lot 2	this paper*
"	"	MA1066	0.2 - 1.5	polyimide sample, flight lot 3	this paper*
"	"	HX507	0.05 - 1.9	gold optical constants	this paper†
Mar. '96	NSLS	HD2338	2.0 - 6.4	flight lot 4, ±1 and higher orders	in prep
"	"	MB1148	2.1 - 4.9	flight lot 9, ±1 and higher orders	in prep
Aug. '96	ALS	poly	0.06 - .940	polyimide transmission, R. Blake	this paper*
Nov. '96	NSLS	1Au	2.01 - 7.0	gold optical constants, R. Blake	this paper†

2. GOLD OPTICAL CONSTANTS

The optical constants for gold have been revised according to the results of three synchrotron tests: two tests (February, 1994 and November, 1996) examined the range above 2 keV, and one (October, 1995) probed energies below 2 keV.

2.1. Gold below 2 keV

In order to investigate the optical constants of gold below 2 keV, transmission tests were made on a free-standing gold sample, HX507, at the radiometry laboratory of the PTB at BESSY. Details of test procedures are given in Flanagan, *et al.*.[8] Information about the facility may be found in Scholze, *et al.*[20] and Ulm and Wende.[21] The gold foil sample contained a residual amount of Cr adhesion layer, and this needed special treatment in the analysis. We assumed Cr optical constants and edge structure as determined according to Section 3.2, and found a best-fit thickness for Cr of 38.7 Å by fitting near the Cr edge features. We then fixed the Cr thickness to this value and fitted over 0.2 to 0.5 keV to obtain a best-fit thickness of 1,075.53 Å for Au. Finally, from the measured transmission, we divided out the contribution due to Cr. Although this left an artifact around 580 eV and did not remove any contribution at the Cr LIII edge (near 696 eV), these effects were comparatively small. The resultant transmission was thus attributed to pure gold of thickness 1,075.53 Å and density 19.3g/cm^3. This yielded the scattering factor f2 directly.

The scattering factor for gold has been independently measured at PTB on a different gold sample by Henneken, *et al.*.[22] These results agree well with our measurements. This is illustrated in Figure 1, where the scattering factor f2 is plotted (from which β is directly obtained) for Henneken's data, for our measurements, and for the Henke values (as updated in 1996). Clearly, the new gold measurements represent a significant difference from earlier values in the range 0.5–1.5 keV. The close agreement between the HETG and Henneken results[22] is illustrated in Figure 2, where the HETG f2 curve is overlaid with Henneken's data and its associated error bars. The HETG results are in

†Section 2
*Section 3

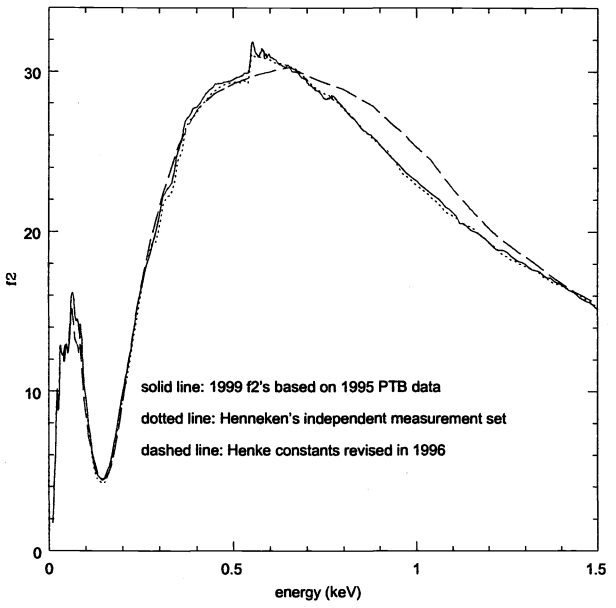

Figure 1. Gold scattering factor f2 obtained from independent transmission measurements by HETG team and Henneken *et al.*,[22] compared with Henke values (updated in 1996). The optical constant β is derived directly from f2 at each energy.

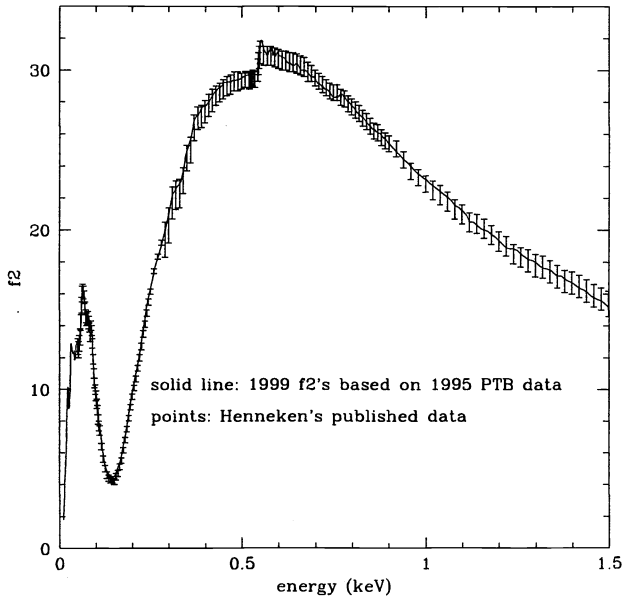

Figure 2. Gold scattering factor f2 obtained by HETG team overlaid with measured values and error bars from Henneken *et al.*[22]

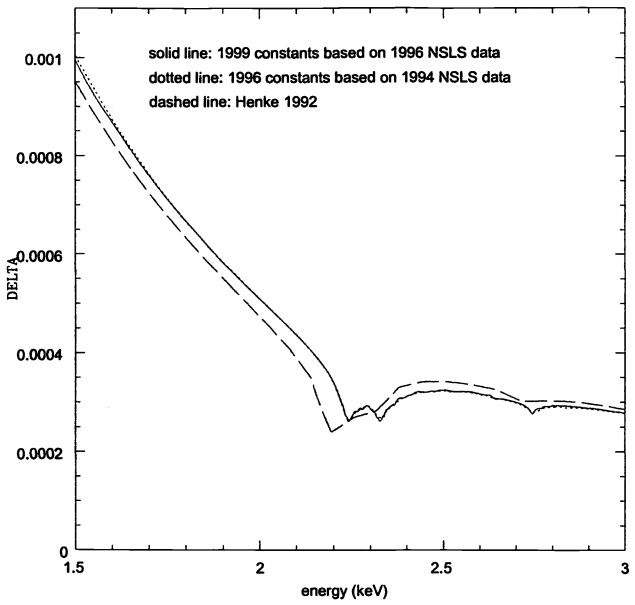

Figure 3. Gold optical constants were revised in May, 1999 for grating modeling. The real part of the index of refraction, δ, is shown here as determined from NSLS 1994 and 1996 measurements, along with Henke 1992 values. The two NSLS results are virtually indistinguishable.

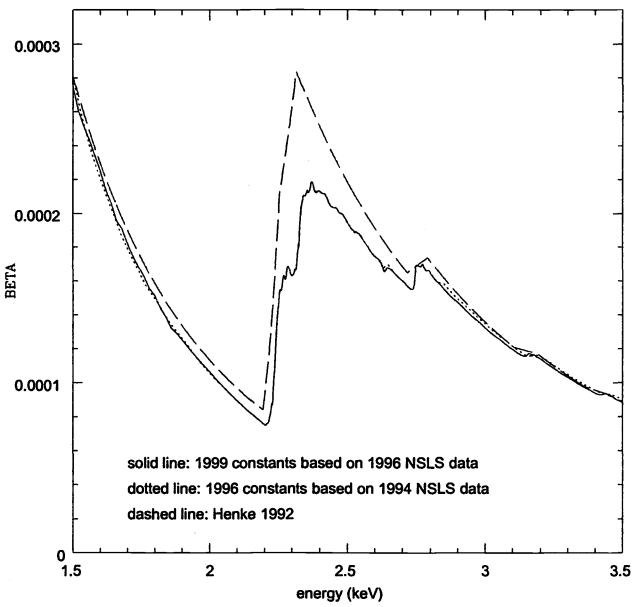

Figure 4. The imaginary part of the index of refraction, β, as determined from NSLS 1994 and 1996 measurements contrasts sharply with Henke 1992 values.

agreement with Henneken's to within the published error bars, except between .13 and .26 keV where the HETG value of f2 is slightly higher (within about 2 σ).

Our data were inadequate below 96 eV, so at this energy we have merged our f2's with those of Henneken's. A complete file of f2 was obtained by joining the measured set from PTB below 2 keV with a newly measured set from NSLS above 2 keV. From this, we generated corresponding f1's for a complete table of scattering factors. All of these revisions are incorporated in the improved grating model.

The impact of the changed gold optical constants on modeling the grating efficiency is small to moderate. Use of the new constants will result in modeled efficiencies that change by five percent or less except at the Au NIII edge near 0.55 keV, where the change is about 7%. There are larger variations at energies below 0.11 keV, but HETG is not intended for use at energies below 0.4 keV for the medium energy gratings (or 0.9 keV for the high energy gratings).

2.2. Gold above 2 keV

The gold sample (1Au) which was measured at NSLS in 1994 was remeasured above 2 keV at NSLS in November, 1996 by Richard Blake and Tony Burek. The assumed thickness was 11,304 Å and the assumed density was 19.32 g/cm^3. In this test, the experimental procedure was improved by continuous beam monitoring and normalizations taken adjacent in time to the transmission measurements. The edges were sampled in 0.5 to 1 eV step sizes. The 1996 data agree well with the 1994 measurements, and have been incorporated into revised optical constants (May 10, 1999). A comparison of the two data sets against Henke[18] values is given in Figures 3 and 4. The two data sets are virtually indistinguishable in the figures. The good agreement between the two measurements of sample 1Au serves to confirm our revisions, and allows a means of assessing some of the errors associated with these measurements.

The largest fractional differences in the two NSLS measurements of β are seen at the gold M edges (in the energy range 2.2 to 3.5 keV), but even there agreement between the two data sets is within 2% (or 4% at the MV edge around 2.2 keV). This corresponds to a 2–3% error in first order efficiency at the gold M edges. Since these two tests were performed on the same beamline, other systematic effects may not be accounted for.

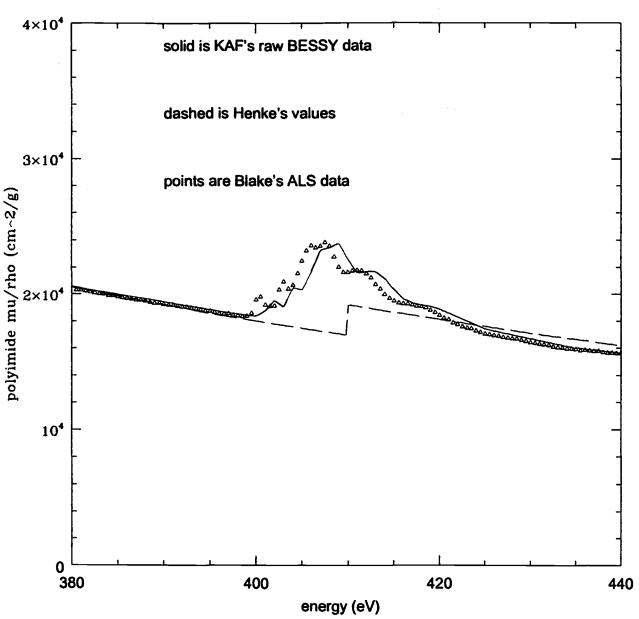

Figure 5. Comparison of polyimide absorption coefficients of the nitrogen edge region at PTB and ALS with Henke values (which represent the HETG model prior to the 1999 revision). The Henke values do not reproduce the complicated edge structure of the HETG polyimide.

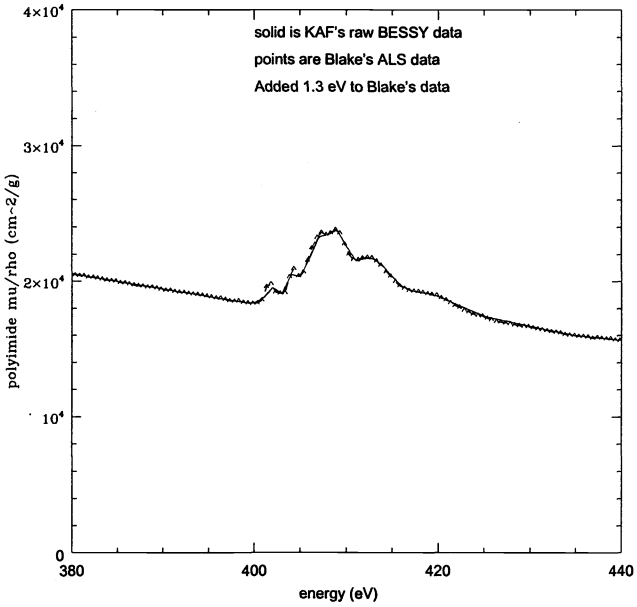

Figure 6. Comparison of PTB nitrogen edge data with ALS data, after an energy shift of 1.3 eV has been applied to the ALS data to accomodate a presumed beamline energy offset. Note that the structure and amplitude of the edge region is confirmed by the two independent beamline measurements.

3. POLYIMIDE AND CHROMIUM EDGE STRUCTURE

3.1. C, N and O Edges

Measurements of the gold optical constants have enabled the detailed gold edge structure to be well represented. A similar approach has been taken toward modeling the C, N and O edges of the polyimide. We have tested samples of polyimide from MEG and HEG flight batches at the radiometry laboratory of the PTB at BESSY.[8] These data show that there is considerable edge structure at the C, N and O edges in our polyimide. Our approach is to model the polyimide assuming the chemical formula ($C_{22}H_{10}O_4N_2$) and nominal density (1.45 g/cm^3) for the polyimide formulation we use (Dupont 2610). In prior modeling, the optical constants for the polyimide support film and the chromium plating base have been based on scattering factors for the constituent atoms taken from Henke, Gullikson and Davis.[18] This modeling, however, provided an unacceptable fit at the edges, with residuals up to 200% at the C and N edges in fitting polyimide transmission data. Just below 600 eV are seen edge residuals on the order of 20% from Cr L in fitting HEG grating data. Similar results have been found for the MEG grating MA1047. Taking the model as a whole, the polyimide edges have exhibited the worst discrepancies between our model and the data overall. As discussed below, synchrotron testing has allowed improvements in our modeling of these edges, although they remain the largest contributors to the errors of the model.

3.1.1. Nitrogen edge

In order to refine the optical constants for our polyimide at the C, N and O edges, we used the PTB data for two flight batch samples of polyimide, HA2049 and MA1066. We began by finding a best-fit thickness for each of the (MEG and HEG) polyimide samples assuming Henke optical constants and fitting over the edge-free energy range 0.6 to 1.6 keV. For each sample, an effective absorption coefficient μ was obtained assuming $T = e^{-\mu t}$ where t is the thickness in microns and T is the transmission through the polyimide membrane. The final value for μ was taken to be the average value of the HEG and MEG μ, between 272 eV and 875 eV, smoothly joined to the Henke values outside this region. In addition, we smoothed the derived μ in the carbon edge region between 288.8 eV and

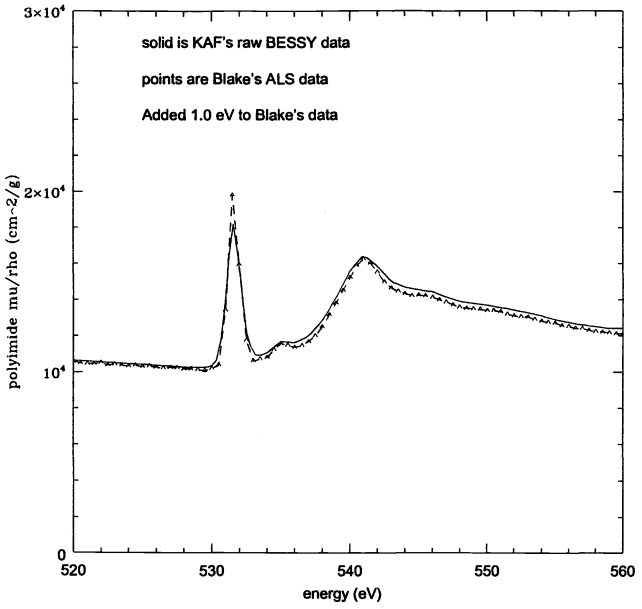

Figure 7. Comparison of PTB oxygen edge data with ALS data, after an energy shift of 1.0 eV has been applied to the ALS data. Note the substantial agreement of the two sets of absorption coefficients, confirming the double structure of the oxygen edge region.

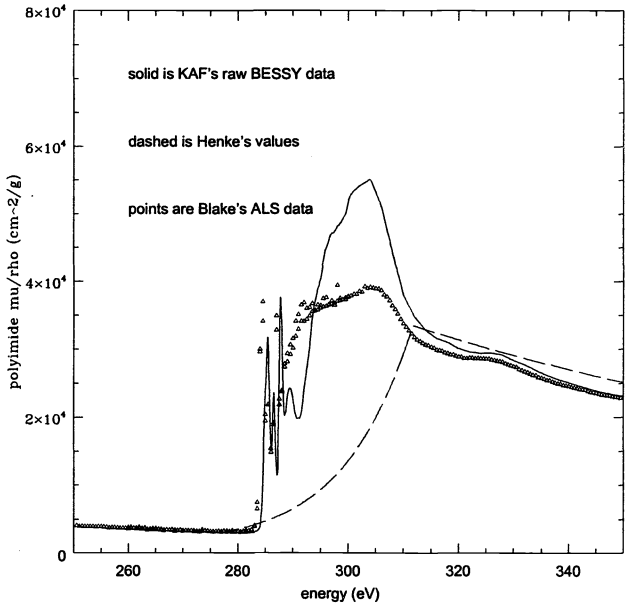

Figure 8. Comparison of PTB carbon edge data with ALS data and Henke values.

300.99 eV because of the jittery structure there. (Although this structure might be real, the low counting statistics and limitations of the experiment discourage reliance on it.) Note that the 1982 Henke constants for carbon were employed in our initial fitting as these were found to agree better with our data and have been shown in independent tests (M. Zombeck, private communication) as the the better choice.

A different polyimide sample, manufactured with the same formulation, was tested at the Advanced Light Source (ALS) at the Lawrence Berkeley National Laboratory in 1996. We found a best-fit ρt of 124.25 $\mu g/cm^2$. Assuming a density of ρ= 1.45 g/cm^3, we derived a value for μ/ρ in a similar manner as has been described with regard to the PTB data. After conversion to comparable units, a comparison of μ/ρ from PTB, from ALS and from Henke[18] is given for the nitrogen edge in Figure 5. As seen in the figure, the Henke values represent the nitrogen edge by a single simple discontinuity, in sharp contast to the measured structure. The PTB and ALS measurements appear to be compatible if one accounts for an apparent slight energy shift (which we attribute to an energy offset in the ALS beamline.) This is shown in Figure 6, where a relative shift of 1.3 eV has been included. The two different beamlines independently trace virtually the same structure and amplitude in this region, giving confidence in the result.

3.1.2. Oxygen edge

Analogous plots of the absorption coefficient in the oxygen edge region are given in Figure 7, where a 1.0 eV energy offset attributed to the ALS beamline has been removed. Note that the Henke representation, which corresponds to our former modeling, cleanly misses the sharp double structure. This structure is accomodated by our updated optical constants. The close agreement generally confirms the detailed edge structure and magnitudes of the absorption coeficients we have derived.

3.1.3. Carbon edge

In general, there was good agreement between the two polyimide data sets (at BESSY and ALS), except at the carbon edge (see Figure 8). Synchrotron beamlines have notorious difficulty with measurements near the carbon edge. (Carbon buildup on the monochromator absorbs much of the incident flux, heightening the relative percentage of contaminant energies, and giving low overall counting statistics.) As discussed above, we take our carbon edge

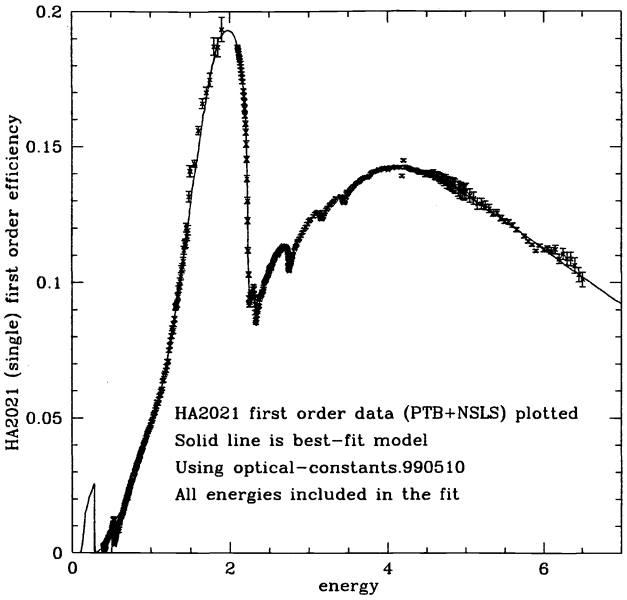

Figure 9. First order synchrotron data of flight batch HEG grating HA2021, overlaid with best fit model. These data come from two different synchrotrons (PTB and NSLS) to cover the full energy span. The data sets join at 2 keV.

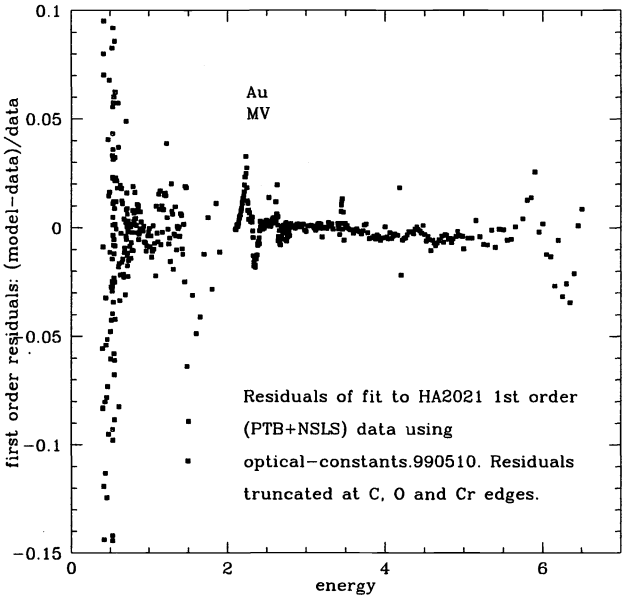

Figure 10. Residuals from the first order fit of grating HA2021 shown in Figure 9. The largest residuals, at the N and O edges of polyimide, have been truncated. (The region containing the N and O edges is detailed in Figures 11 and 12.)

structure from the PTB measurements, but (arbitrarily) smoothing the data between 288.8 eV and 300.99 eV. We do not have the reassuring agreement between the ALS and PTB measurements for this region as we did for the nitrogen and oxygen edges, and model residuals remain high at the carbon edge. However, this region falls below the minimum HETG energy of 400 eV and the true edge structure does not matter for our modeling purposes.

3.2. Chromium edge

In order to accomodate the Cr edge structure below 600 eV, we employed a different approach since we do not have transmission tests of a Cr filter of known thickness. We took zero order grating data from MA1047 (measured at PTB) and fit it assuming a fixed thickness of Cr (55 Å from fabrication measurements). We assumed that the absorption features seen at 577 eV and 586 eV could be modeled as a perturbation on the absorption coefficient as derived from the Henke constants, and thereby obtained a modified absorption coefficient. This allows us to obtain a transmission for any thickness of Cr. (It is unnecessary to extract new values of f1, since the chromium absorbs but does not diffract.)

The updated grating model is evaluated in the next section. By refining our treatment of C, N, O and Cr edges, we have reduced the residuals by a factor of 2–3 relative to the former treatment.

4. ACCURACY OF THE GRATING MODEL

4.1. Overview

The accuracy of the phased, non-rectangular model and the effectiveness of updated optical constants for gold, polyimide and chromium can be assessed by examining how well the model fits the measured efficiencies of a well-tested grating. There are two flight-batch gratings that have been tested at synchrotrons over most of the applicable energy range. These gratings are MA1047 and HA2021, which were tested at in October, 1995 at PTB below 2 keV, and at NSLS above 2 keV. (Although other gratings have been through synchrotron testing, the experiment was limited to energies above 2 keV for these other gratings.) As discussed below, the grating model shows excellent

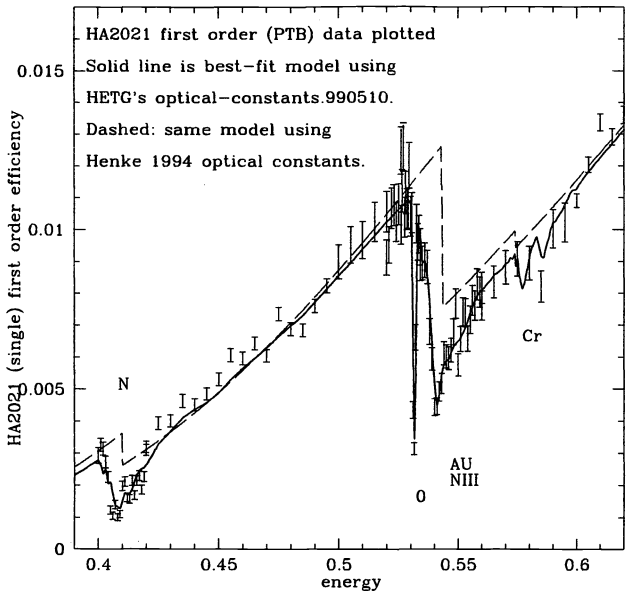

Figure 11. First order synchrotron data of HEG grating HA2021 overlaid with best fit model, in the polyimide and plating base edge region. The contrast between the current model (solid line) and the 1994 Henke model (dashed line) illustrates the remarkable level of improvement provided by the polyimide and gold transmission tests at the synchrotrons.

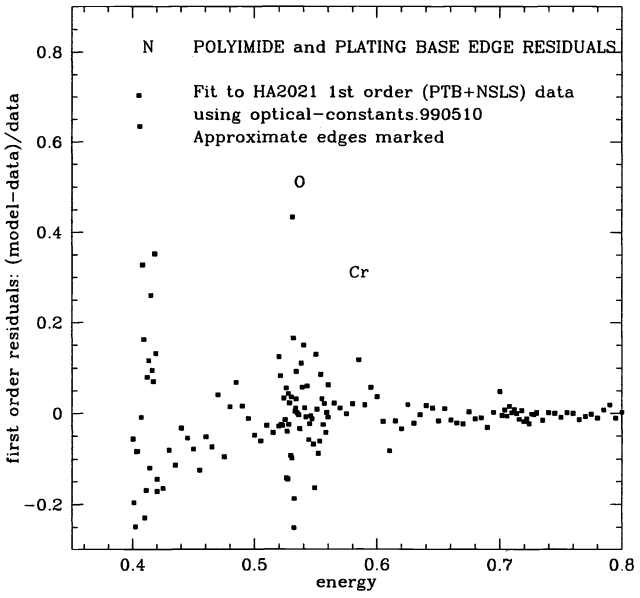

Figure 12. Residuals from the first order fit of grating HA2021, in the polyimide and plating base edge region. Although the residuals at the N and O edges are high, they are nevertheless significantly improved by the use of the new optical constants.

agreement (at the level of a few percent) with synchrotron measurements of first order efficiencies, except at a limited set of energies. In particular, modeling the edges remains the largest contributor to the residuals, despite significant advances in this area. Future work on the modeling is not expected to improve the edge residuals. The second obvious energy range where the model inadequately represents the data is in the vicinity of the first order efficiency peak (or zeroth order efficiency trough). Future work on the modeling may result in improvements in this energy range.

4.2. First order fit to HA2021

The agreement between the model and the data is demonstrated in Figure 9, where first order diffraction efficiencies for flight-batch grating HA2021 have been measured at many closely-spaced energies. The residuals are shown in Figure 10, where have defined the residuals to be the fractional discrepancy between the modeled efficiency and the data (i.e. $(model - data)/data$) without consideration of the error bars on the data. To obtain the best-fit model, only the first-order data for HEG grating HA2021 were used in the fit. (No other orders were used, nor did we impose the constraint that the +1 and -1 orders were equal.) The largest residuals are generally due to the polyimide and plating base edges, and have been truncated in Figure 10. Detailed views of the model and the residuals in this energy region are given in Figures 11 and 12. The excellent agreement of the model with the data at the gold M edges is seen in detail in Figures 13 and 14.

By far the largest residuals (tens of percent) between the model and the data occur at the polyimide edges (N and O). (The testing range did not include the carbon edge.) Given the steep changes in response expected there and the large systematic errors found in measuring the polyimide optical constants at independent synchrotron beamlines,

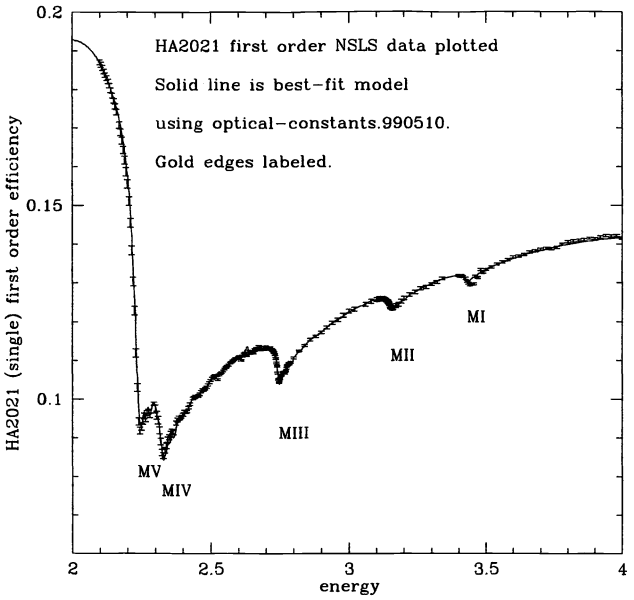

Figure 13. First order synchrotron data of HEG grating HA2021 overlaid with best fit model, in the gold M edge region.

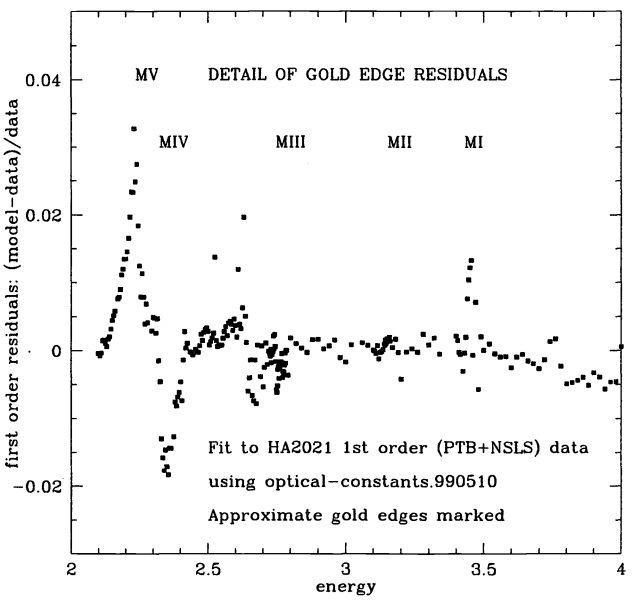

Figure 14. Residuals from the first order fit of grating HA2021, in the gold M edge region. Note that the residuals are small, a few percent at most.

these residuals are perhaps not too surprising and are restricted to a relatively small region of the energy range. (Furthermore, the residuals as we have defined them do not include any impact of the error bars in evaluating the significance.) A close examination of Figure 11, in fact, shows that the model is actually quite impressive in its treatment of the complicated edge structures, despite the formal residuals.

Figure 15 summarizes the model to the first order data of HA2021. The model to which the data are fitted is a five-vertex polygon bar shape function with three absorbing layers: polyimide, chromium, and gold plating base. For HA2021, the nominal fabrication thicknesses are 0.0200 μm for the Au plating base, 0.97 μm for polyimide, and 0.005 μm for Cr. The fitted values are displayed in Figure 15, and are in the ballpark of the expected values. Also shown is the amplitude factor: it close to 1.0, as expected.

As indicated in Figure 15, the reduced chisquare of the fit shown in Figure 9 is about 3. Part of this is attributable to error bars that are too small. If the statistical errors from the synchrotron tests are increased in order to more realistically reflect systematic errors, then the reduced chisquare drops to 2.1, but not much lower. (The edge regions continue to be significant contributors.) Thus, despite improvements gained with the recent synchrotron tests, there still remain some discrepancies between the model and the data, mostly attributable to limitations in our input data, β and δ over the edge regions.

Table 2 shows the improvement that polyimide and gold transmission tests have provided in understanding the optical constants at these edges. The improvement in the optical constants at the edges has decreased the relative residuals (improvements of a factor of 2 or 3 are typical). Note that in Table 2, most of the edges fall outside the useable energy range of the high energy grating (above 0.9 keV). Thus, from the standpoint of *Chandra* calibration, the largest applicable edge residual is 26% (i.e., the MEG grating at the oxygen edge.) Future improvements in modeling are not expected to improve the edge residuals, since these are assumed due to systematics in the synchrotron testing, location of the edge energy, variations in polyimide, and other factors outside our ability to address. (Further improvements in our treatment of the edges must await improved optical constants in these regions.) We can, however, further examine the model at the conceptual level, as discussed below.

A perusal of Figure 9 shows two regions where the model fit does not agree well (systematically) with the data. One region is about 6 keV. This is probably due to inadequate separation of the first order from the zeroth order in the synchrotron test, and is therefore a fault of the test rather than a failure of the model. The second region is the

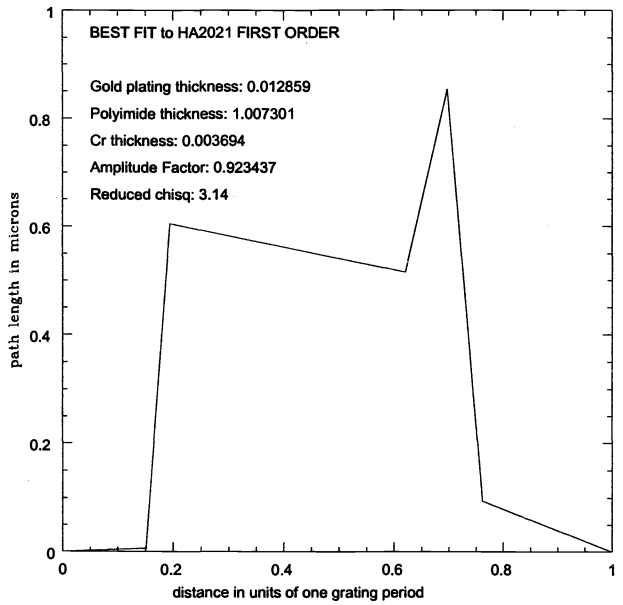

Figure 15. Summary of the best-fit model to the first order data of HA2021. The model includes a five-point vertex bar shape, three plating base thicknesses, and an amplitude factor.

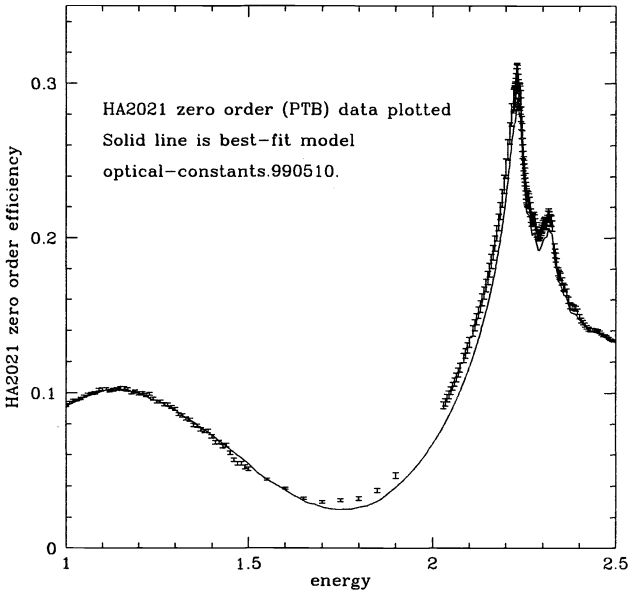

Figure 16. Zero order synchrotron data of flight batch HEG grating HA2021, overlaid with the best fit model. The region around the "trough" is highlighted to illustrate where conceptual improvements may be made in the grating model.

Table 2. Typical edge residuals (percent)

Asterisk marks energies outside the applicable range for the gratings.

Model Year	Grating	N	O	Cr	MV
1999	MA1047	13	26	4.3	1.6
1996	MA1047	42	66	13	2.7
1999	HA2021	70*	43*	12*	3.3
1996	HA2021	93*	114*	28*	5.6

low-energy side of the efficiency peak (about 1.5 to 2 keV). This region is also poorly fit for zeroth order, as shown in Figure 16. The reasons for the poor fit over the resonance peak (and conversely in the resonance trough of the zeroth order) are not known, although several possibilities may be considered.

The region near 2 keV corresponds to the energies in which the xray undergoes nearly a 180 degree phase shift after traversing the grating bar. This phase shift results in a near cancellation of the emerging xray wavefront in zeroth order and an enhanced first order efficiency. Hence this region is extremely sensitive to the detailed bar shapes and any attempt to model the shapes as a single shape may ultimately fall short. In fact, we believe that the unusual bar shape depicted in Figure 15 is indicative of this fact as its distorted shape will give rise to a complex pattern of phase shifts. Similarly modeling the grating efficiency as a linear combination of efficiencies from different bar shapes may also not provide an improved fit because this technique does not account for interference effects. In other words, this energy regime may be impossible to model at the desired level of accuracy using a model based upon diffraction

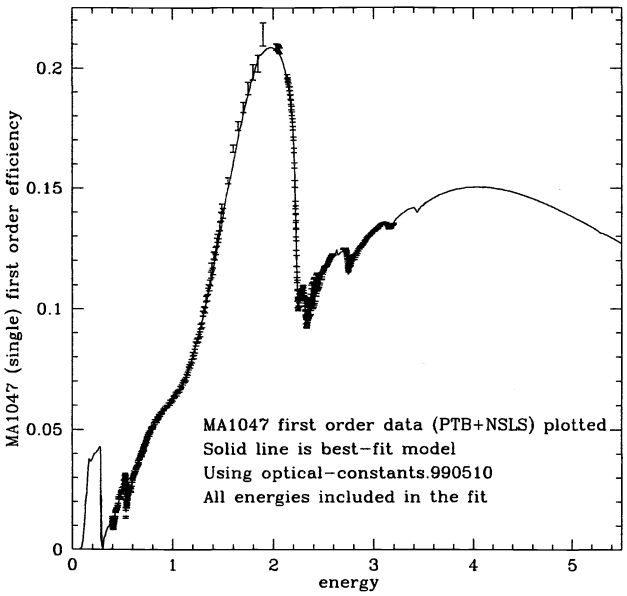

Figure 17. First order synchrotron data of flight batch MEG grating MA1047, overlaid with the best fit model. These data come from two different synchrotrons (PTB and NSLS) to cover the full energy span. The data sets join at 2 keV. Only first order data have been included in the fit.

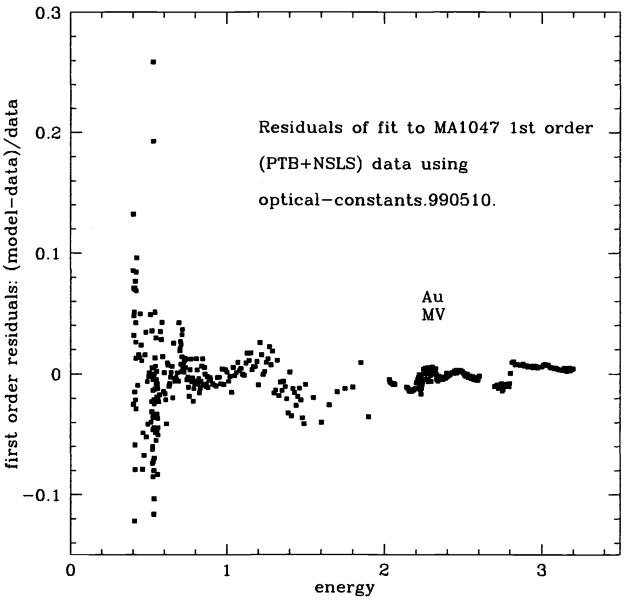

Figure 18. Residuals from the first order fit of grating MA1047 shown in Figure 18. Residuals have not been truncated.

from a periodic structure, or a superposition of periodic structures.

Other possible explanations may also be considered:

- The peak of the efficiency curve (2 keV) is also the energy where the data from the different synchrotrons meet. The actual location tested on grating HA2021 may be slightly different in the two tests, so that in effect two different gratings are being inappropriately represented by a single model. This should be easy to verify by individually modeling the two energy regions.
- The PTB beamline is known to have stray light contamination above 1500 eV, and this may affect the quality of the data being fitted in the peak.
- Since macroscopic areas of the grating are illuminated in the synchroton tests, it may be appropriate to assume more than one grating thickness. This might be expected to broaden the efficiency peak overall. Simple models with two thicknesses have *not* been found to significantly improve the model fit in this region, however.
- It may be necessary to abandon the scalar theory altogether in favor of the much more complex vector theory that includes the effects of polarization.
- The amplitude factor should probably vary with energy.

Thus, it is possible that improvements in the grating model at the conceptual level (i.e., vector model, multiple thicknesses, etc.) may improve the fit around the first order efficiency peak.

4.3. First order fit to MA1047

A fit to the first order efficiency of MEG flight batch grating MA1047 is shown in Figure 17. The residuals are shown in Figure 18, and have similar characteristic regions to those described for HA2021. In the case of the MEG, the residuals at the polyimide edges are less than for the HEG grating, as expected since the absorbing layer of polyimide is about half that of the HEG grating. Typical results for MA1047 are also given in Table 2.

5. SUMMARY

The grating model shows excellent agreement (at the level of a few percent) with synchrotron measurements of first order efficiencies, except at a limited set of energies. In particular, the edges remain the largest contributor to the residuals, although our modeling of the edge structures has improved dramatically. Our measurements at PTB and NSLS have gone far to improve the optical constants β and δ which are inputs to our model. Future efforts will be directed at conceptual improvements in the model; in particular, the resonance peak around 2 keV represents one area that invites further investigation.

ACKNOWLEDGMENTS

We thank the HETG and CXC groups for helpful suggestions, in particular C. Canizares, D. Davis, D. Dewey, J. Houck, H. Marshall, S. Taylor and T.T. Fang. We are grateful to T. Burek for assistance in gold transmission tests. This work was prepared under NASA contract NAS8-38249.

REFERENCES

1. T.H. Markert, C.R. Canizares, D. Dewey, M. McGuirk, C. Pak, and M.L. Schattenburg, "The High Energy Transmission Grating Spectrometer for AXAF", in *EUX, X-Ray, and Gamma-Ray Instrumentation for Astronomy V*, O.H.W. Siegmund and J.V. Vallerga, eds., *Proc. SPIE* **2280**, pp. 168–180, 1994.
2. M.L. Schattenburg, R.J. Aucoin, R.C. Fleming, I. Plotnik, J. Porter, and H.I. Smith, "Fabrication of High Energy X-ray Transmission Gratings for AXAF", in *EUX, X-Ray, and Gamma-Ray Instrumentation for Astronomy V*, O.H.W. Siegmund and J.V. Vallerga, eds., *Proc. SPIE* **2280**, pp. 181–190, 1994.
3. D.Dewey, D.N. Humpheries, G.Y. McLean and D.A. Moschella, "Laboratory Calibration of X-ray Transmission Diffraction Gratings", in *EUX, X-Ray, and Gamma-Ray Instrumentation for Astronomy V*, O.H.W. Siegmund and J.V. Vallerga, eds., *Proc. SPIE* **2280**, pp. 257–271, 1994.
4. K.A. Flanagan, D. Dewey, L. Bordzol, "Calibration and Characterization of HETG grating elements at the MIT X-ray Grating Evaluation Facility", in *EUX, X-Ray, and Gamma-Ray Instrumentation for Astronomy VI*, O.H.W. Siegmund and J.V. Vallerga, eds., *Proc. SPIE* **2518**, 438–456 (1995).
5. C.S. Nelson, *Synchrotron Studies of an X-ray Transmission Grating*, Bachelor's Thesis, Massachusetts Institute of Technology, 1994.
6. C.S. Nelson, T.H. Markert, Y.S. Song, M.L. Schattenburg, K.A. Flanagan, R.L. Blake, J. Bauer, E.M. Gullikson, "Efficiency Measurements and Modelling of AXAF High Energy Transmission Gratings", in *EUX, X-Ray, and Gamma-Ray Instrumentation for Astronomy V*, O.H.W. Siegmund and J.V. Vallerga, eds., *Proc. SPIE* **2280**, pp. 191–203, 1994.
7. T.H. Markert, D. Dewey, J.E. Davis, K.A. Flanagan, D.E. Graessle, J.M. Bauer, C.S. Nelson, "Modeling the Diffraction Efficiencies of the AXAF High Energy Transmission Gratings", in *EUX, X-Ray, and Gamma-Ray Instrumentation for Astronomy V*, O.H.W. Siegmund and J.V. Vallerga, eds., *Proc. SPIE* **2518**, pp. 424–437, 1995.
8. K.A. Flanagan, T.T. Fang, C. Baluta, J.E. Davis, D. Dewey, T.H. Markert, D.E. Graessle, J. Drake, J.E. Fitch, J.Z. Juda, J. Woo, S. Kraft, P. Bulicke, R. Fliegauf, F. Scholze, and G. Ulm, "Modeling the Diffraction Efficiencies of the AXAF High Energy Transmission Gratings: II", in *EUX, X-Ray, and Gamma-Ray Instrumentation for Astronomy VII*, O.H.W. Siegmund and M.A. Gummin, eds., *Proc. SPIE* **2808**, pp. 650–676, 1996.
9. D. Dewey, H.L. Marshall, K.A. Flanagan, C. Baluta, C.R. Canizares, D.S. Davis, J.E. Davis, T.T. Fang, D.P. Huenemoerder, J.H. Kastner, N.S. Schulz, M.W. Wise, J.J. Drake, J.Z. Juda, M. Juda, A.C. Brinkman, T. Gunsing, J. Kaastra, G. Hartner and P. Predehl, "Towards the Callibration of the HETG Effective Area", in *Grazing Incidence and Multilayer X-Ray Optical Systems*, R.B. Hoover and A.B.C. Walker, eds., *Proc. SPIE* **3113**, pp. 144–159, 1997.
10. D. Dewey, J.J. Drake, R.J. Edgar, K. Michaud, and P. Ratzlaff, "AXAF Grating Efficiency Measurements with Calibrated, Non-imaging Detectors", in *X-Ray Optics, Instruments, and Missions*, R.B. Hoover and A.B.C. Walker, eds., *Proc. SPIE* **3444**, pp. 48–63, 1998.
11. K.A. Flanagan, N.S. Schulz, S.S. Murray, G.D. Hartner, and P. Predehl, "HETG High-order Diffraction Efficiency" in *X-Ray Optics, Instruments, and Missions*, R.B. Hoover and A.B.C. Walker, eds., *Proc. SPIE* **3444**, pp. 106–126, 1998.

12. H.L. Marshall, D. Dewey, K.A. Flanagan, C. Baluta, C.R. Canizares, D.S. Davis, J.E. Davis, T.T. Fang, D.P. Huenemoerder, J.H. Kastner, N.S. Schulz, M.W. Wise, J.J. Drake, J.Z. Juda, M. Juda, A.C. Brinkman, C.J.Th. Gunsing, and J.S. Kaastra, G. Hartner and P. Predehl, "Towards the Calibration of the HETGS Line Response Function", in *Grazing Incidence and Multilayer X-Ray Optical Systems*, R.B. Hoover and A.B.C. Walker, eds., *Proc. SPIE* **3113**, pp. 160–171 (1997).
13. H.L. Marshall, D. Dewey, N.S. Schulz, and K.A. Flanagan, "Spectral Features in the AXAF HETGS Effective Area using High-signal Continuum Tests", in *X-Ray Optics, Instruments, and Missions*, R.B. Hoover and A.B.C. Walker, eds., *Proc. SPIE* **3444**, pp. 64–75, 1998.
14. N.S. Schulz, D. Dewey, H.L. Marshall, "Absolute Effective Areas of HETG", in *X-Ray Optics, Instruments, and Missions*, R.B. Hoover and A.B.C. Walker, eds., *Proc. SPIE* **3444**, pp. 160–176, 1998.
15. J.E. Davis, H.L. Marshall, M.L. Schattenburg, and D. Dewey, "Analysis and Modeling of Anomalous Scattering in the AXAF HETGS", in *X-Ray Optics, Instruments, and Missions*, R.B. Hoover and A.B.C. Walker, eds., *Proc. SPIE* **3444**, pp. 76–92, 1998.
16. H.L. Marshall, "High Resolution X-Ray Imaging and Spectroscopy of AGN and SS433 with the Chandra X-Ray Observatory," in *Astrophysical Phenomena Revealed by Space VLBI*, H. Hirabayashi, P.G. Edwards and D.W. Murphy, eds., pp. 207–214, 2000.
17. M. Born and E. Wolf, *Principles of Optics, Sixth Ed.*, Pergamon, New York, pp. 401–414, 1980.
18. B.L. Henke, E.M. Gullikson, and J.C. Davis, "X-ray Interactions: Photoabsorption, Scattering, Transmission, and Reflection at E = 50–30,000 eV, A = 1–92", *Atomic Data and Nuclear Data Tables*, **54**, No. 2, July 1993.
19. R.L. Blake, J.C. Davis, D.E. Graessle, T.H. Burbine, and E.M. Gullikson, "Optical Constants and Scattering Factors from Reflectivity Measurements: 50 eV to 5 keV", in *Journal of X-ray Science and Technology*, in press.
20. F. Scholze, M. Krumrey, P. Müller, and D. Fuchs, *Rev. Sci. Instrum.* **65**, p. 3229, 1994
21. G. Ulm, B. Wende, *Rev. Sci. Instrum.* **66**, pp. 2244–2247, 1995.
22. H. Henneken, F. Scholze, and G. Ulm, "Lack of proportionality of total electron yield and soft x-ray absorption coefficient", *J. Appl. Phys.*, **87**, No.1, pp. 257–268, 2000.